

DESIGN OF A DYNAMICALLY SCALED ROTOR SYSTEM AND VERIFICATION OF THE BLADE PROPERTIES

Do-Hyung Kim* and Seung-Ho Kim

Rotor Department, Rotorcraft Program Office, Korea Aerospace Research Institute (KARI),
45 Eoeun-dong, Yuseong-gu, Daejeon 305-333, Republic of Korea

* dhkim@kari.re.kr

ABSTRACT

A dynamically and mach scaled rotor system was designed for performance evaluation of a utility helicopter. After fabrication of the model blade, verification of the blade properties was performed through simple laboratory tests. Cross sectional stiffness was measured using strain gauges, and mass and c.g. offset were measured using sliced pieces. Then modal frequencies at cantilevered condition were evaluated. The measured sectional properties were compared with designed values, and blade modal frequencies at non-rotating condition using designed and measured values were compared. And the effects of mass and stiffness differences on non-rotating and rotating frequencies were investigated.

INTRODUCTION

In the development of new rotorcraft, model-scale rotor systems are often utilized to verify a candidate design. The use of model-scale rotors to achieve this design verification is cost effective and also permits a much easier variation of model parameters to conduct design studies and optimizations [1, 2]. For the performance testing at model scale, matching the full-scale tip Mach number is required to duplicate compressibility effects and also to minimize the reduction in Reynolds number [2]. It is also indicated that the Reynolds number effects might be the same magnitude or smaller than rotor solidity and blade elastic properties in rotor aerodynamic performance testing [3]. Model-scale rotor system does not exactly represent full-scale rotor's characteristics, not just because the differences in scaling parameters including Mach number and Reynolds number. Numerical scaling down of a full-scale rotor system can produce ideally scaled model system, but there are many uncertainties and limitations in design and fabrication processes. Therefore the evaluation of the fabricated model's properties is essential process for the construction of model-scale rotor system.

The wind tunnel test is the final test for a model system. In the wind tunnel test, finally the dynamic

characteristics of the model rotor system will be identified. In case the analytical model of a rotor system has to be adapted to the prediction of the wind tunnel measurement, it is necessary to verify the analytical model prior to the prediction of wind tunnel test condition. Therefore the model-scale rotor system should be checked through various test steps in order to define cross sectional properties such as bending stiffness, torsion stiffness, mass distribution, and so on.

In this study, a dynamically and Mach scaled rotor system was designed for performance evaluation of a utility helicopter. After fabrication of the model blade, verification of the model blade properties was performed through laboratory tests. For the measurement of bending stiffness, relations between applied moment and deflection or slope could be used. However measurement of deflection or slope is difficult for a small scaled model blade in small deflection. In addition, slight error in measurement of deflection or slope can result in large error in extracted bending stiffness. Compared to deflection or slope, strain can be sensitively measured using strain gauges even for a small deflection case. Therefore the relation between applied moment and surface strain was utilized for the verification of bending stiffnesses. And then, the acquired sectional properties were

compared with designed values, and it was used for the calculation of the modal frequencies at non-rotating condition. The designed model and revised model using test data were compared with tested modal frequencies. Finally, the analytical model was updated for representing manufactured model-scale rotor system. And then the effects of model update on the rotating frequencies were investigated; the fanplot of the updated model has been calculated and compared with target and designed models. The updated model will be used for the analysis of wind tunnel test condition.

SCALED-MODEL DESIGN

Scaling of the rotor system has been performed within the limitation of the test facilities; mainly considering the configuration and capability of Korea Aerospace Research Institute Low-Speed Wind Tunnel (KARI LSWT) and the rotor test stand. From the evaluation of several parameters such as required power, rotating speed and rotor diameter, 1/7 scale was selected for the model scaling factor. At first, the target model is constructed by scaling from the full-scale rotor system; the dynamic characteristics of the target model are identical to those of the full-scale model.

Blade Cross Section Design

The model blade was dynamically scaled in a way such that natural frequencies were matched with the full-scale behavior for the first three flapping modes, the first two lead-lag modes and the first torsion mode.

Blade cross section design has been performed to match the target model's sectional properties. Twelve typical sections (S1~S12) were designed with D-spar shape using KARI's in-house program, CORDAS (Composite Rotor blade Design and Analysis Software) [4]. Radial stations for cross section design are shown in figure 1.

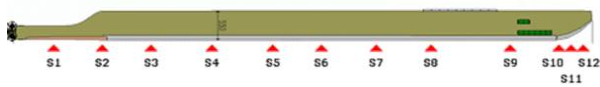


Figure 1. Radial stations for section design.

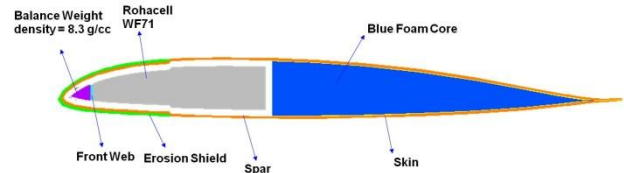
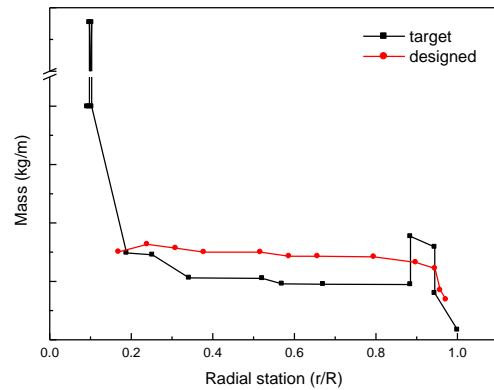


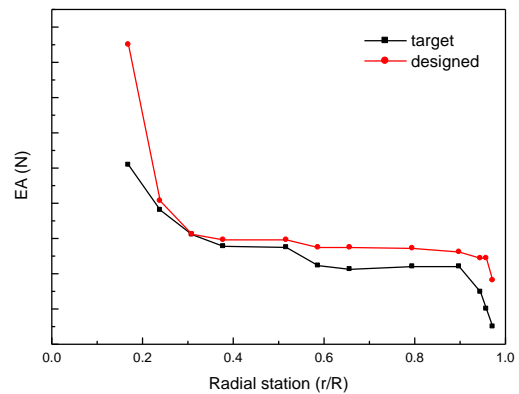
Figure 2. Typical section view of model blade.

Typical section view of designed blade is shown in figure 2. It consists of carbon erosion shield, skin, spar, balance weight, front web, spar foam core and trailing edge foam core. Carbon/epoxy prepreg (HT145/RS1222, Hankuk Fiber) is used for spar, and carbon fabric (HPW193/RS1222) is used for skin.

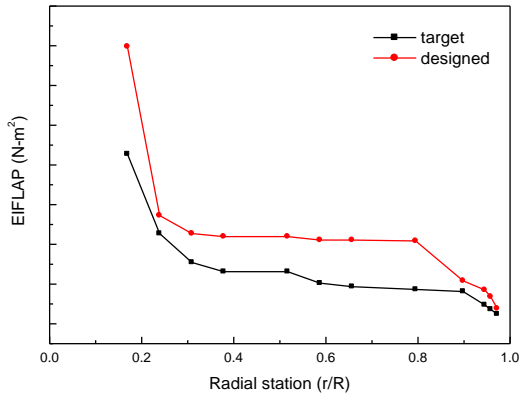
The designed radial distribution of the sectional properties is not exactly same to the properties of target model. Slightly higher stiffness was preferred because possible mass distribution is higher than numerically scaled target values. The sectional properties for the target and the designed values are compared in figure 3.



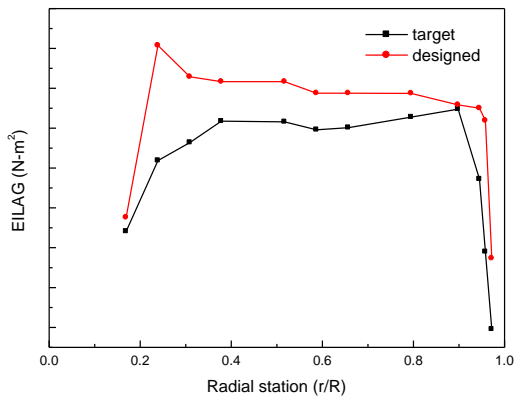
(a) mass



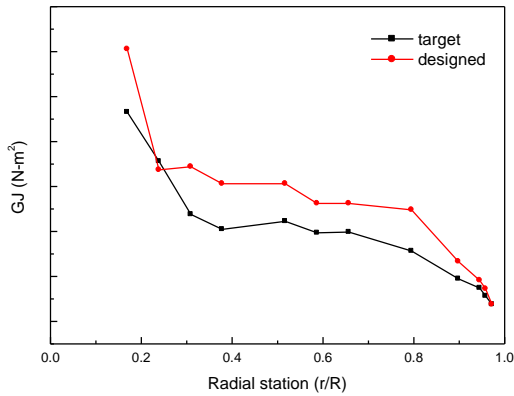
(b) axial stiffness



(c) flap bending stiffness



(d) lag bending stiffness



(e) torsional stiffness

Figure 3. Sectional properties of scaled blade.

In order to check the dynamic characteristics, rotating frequencies of target and designed model are compared in figure 4. Lowest three modes of the designed model are almost same as the target model, and the difference becomes bigger for higher modes.

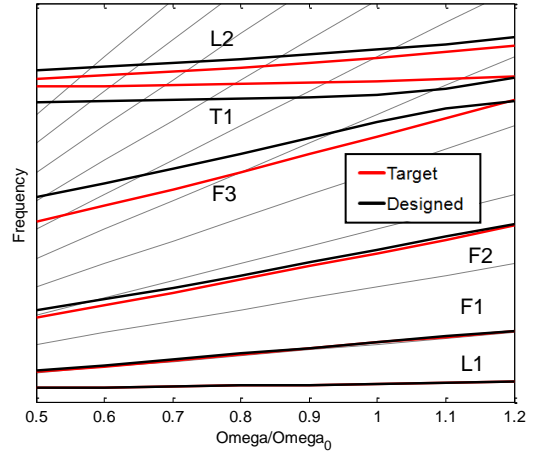


Figure 4. Fanplots of target and designed model.

Hub Design

Scale-down design for the hub is the same as the blade. However it is difficult to implement elastomeric spherical bearing and dampers in very small dimensions. Therefore elastomeric spherical bearings are replaced by mechanical flap/lag hinges and pitch bearings with tension torsion strap. And the simplified stack type elastomeric dampers are adopted. Although elastomeric bearings and dampers are not exactly implemented, the hub structure has identical location of flap/lag hinges and the same pitch-flap coupling angle. Configuration of the hub is shown in figure 5.

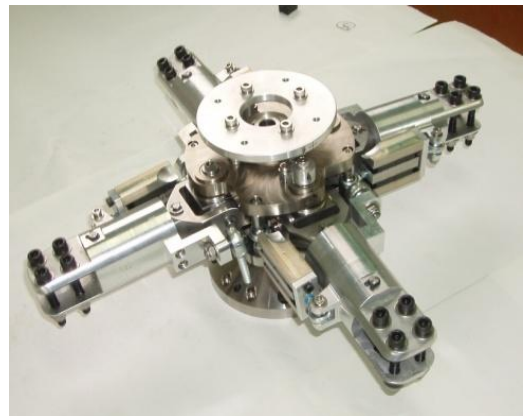


Figure 5. Small-scaled hub system.

Design Load and Static Strength Analysis

For the static structural analysis, load analysis for the level flight condition in wind tunnel was performed. CAMRAD II [5] was applied to the load analysis for flight speeds up to 120 kts.

Static strength of the blade and margin of safety has been calculated at twelve designed locations. For the structural analysis, ultimate load which is 1.5 times design limit load was applied, and margin of safety was calculated based on design allowable strain. Minimum margin of safety is found at S3 location (30.9%R); which is 1.64. Flight condition of this case is 120 kts level flight, and maximum strain was occurred at the lower skin 4.5% chord aft from the leading edge.

Aeroelastic Stability Analysis

For the validation of aeroelastic stability, analysis for the designed model was performed at hover and forward flight condition. When the elastomeric dampers are used, the rotor system at hover shows sufficient modal damping for all collective pitch angle range. For the conservative consideration, modal damping of the rotor system without lead-lag damper in hover was performed; which is shown in figure 6.

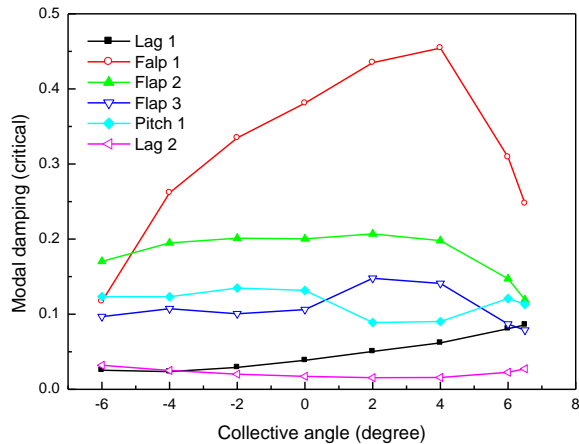


Figure 6. Modal damping of the rotor system without damper in hover.

The 2nd lag mode shows lowest damping, but it is still in the stable condition. And the modal damping of the 1st and 2nd lag modes becomes sufficiently higher values when the elastomeric dampers are adopted.

Modal damping of the rotor system for the forward flight condition does not show significant variation except the first flap mode. Modal damping of the first flap mode shows slightly decrease around 40 kts of flight speed as shown in figure 7.

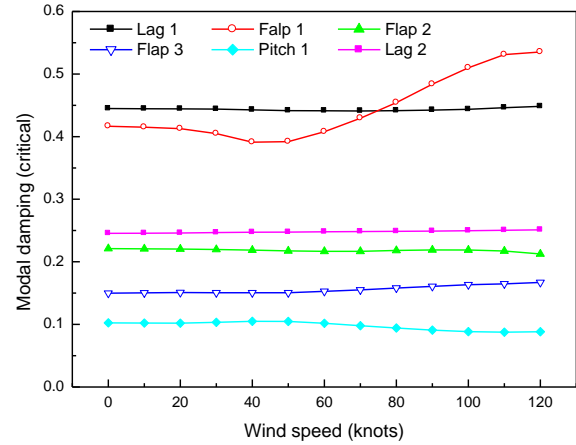


Figure 7. Modal damping of the rotor system with damper in forward flight.

MODEL BLADE VERIFICATION

The composite blade was fabricated based on the design result. Outer surface of the blade was inspected using templates and cross sectional stiffnesses were measured. Then modal frequencies at cantilevered boundary condition were evaluated, and mass and c.g. offset for sliced pieces were also measured.

Bending Stiffness

Strain gauges were used to measure the strain under a defined blade bending moment in flap and lead-lag direction. In regard to the measured strain at the tension side (ϵ_1) and at the compressed side (ϵ_2), one can get the following relationship according to the figure 8.

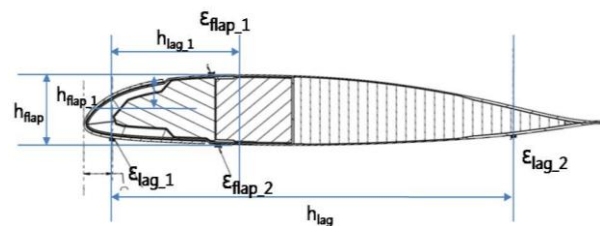


Figure 8. Locations and distances of strain gauges.

$$h_1 = \frac{\epsilon_1 \cdot h}{\epsilon_1 + \epsilon_2} \quad (1)$$

where, h is the distance of the strain gauge pairs in chordwise or flapwise directions, and ϵ_1 , ϵ_2 are measured strains. For an ideal Euler beam, h_1 is the

distance between the neutral axis location and the measurement point for ε_1 .

The measured bending stiffness can be obtained as follows;

$$\varepsilon_1 = \frac{M \cdot h}{EI} \quad (2)$$

where,

$$M = P \times (R - r_i) \quad (3)$$

M is the bending moment at the measured cross section, which is produced by the static load P at the blade tip.

For the measurement of the flap and lead-lag bending stiffnesses of the scaled model blade, strain gauges were installed at nine locations, S1 ~ S9 in figure 1. Outer three locations, S10 ~ S12, of the designed location were not included in the stiffness measurement due to the fixture for applying bending moments. The bending moments were applied by the various weights, and the strain of tension and compression sides were measured. At each location, initial twist angle was adjusted to make the instrumented blade section perpendicular or parallel to the applied load. The configuration of the test is shown in the figure 9.



Figure 9. Flap bending stiffness measurement.

Three weight conditions were used for applying bending moments. Bending stiffnesses were extracted for each case and then averaged for representing bending stiffness. The measured bending stiffness were compared with designed values in figure 10 and figure 11. Measured flap bending stiffness is close to the designed values; however lag bending stiffness shows large deviation

in inboard region, especially S2 location, which is transient area from blade root to airfoil section. Actually cross section of the S2 is airfoil shape; however this is starting location of main airfoil section. The adjacent transient region between S1 and S2 might have more stiffening effects in chordwise direction rather than flapwise direction.

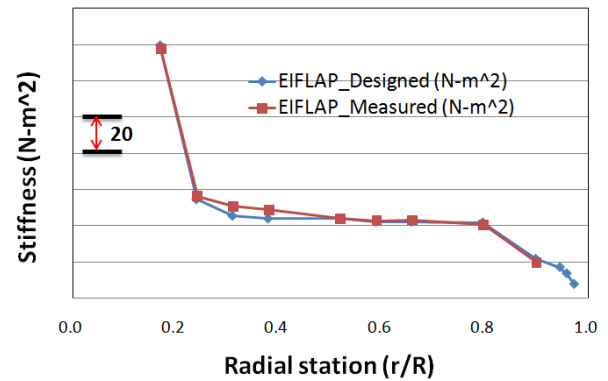


Figure 10. Measured and designed flap bending stiffnesses.

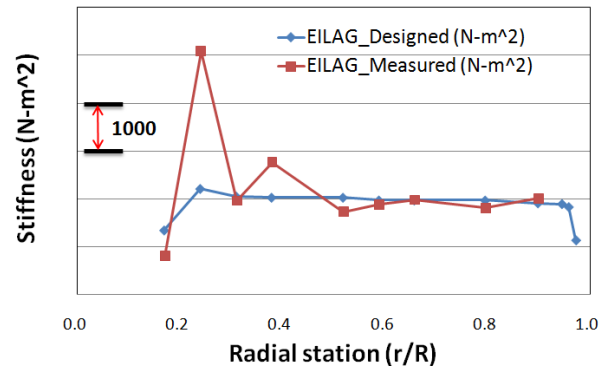


Figure 11. Measured and designed lag bending stiffnesses.

Torsion Stiffness

For the measurement of the torsion stiffness of the blade, the relationship between applied torque and twist angle was used.

$$GJ = (T \cdot L) / \Delta\theta \quad (4)$$

where, T is applied moment, L is the distance from the fixed end to the location of twist angle measurement.

Torsion stiffness was not measured at all designed locations, because precise measurement

of applied moment and twist angle is difficult for small model blade. Small amount of error in twist angle can cause large amount of error in torsion stiffness. Therefore four sections of the blade were considered, and the averaged torsion stiffness of each section was measured just for reference. The torsion stiffnesses of the four sections look similar to the designed values as shown in figure 12.

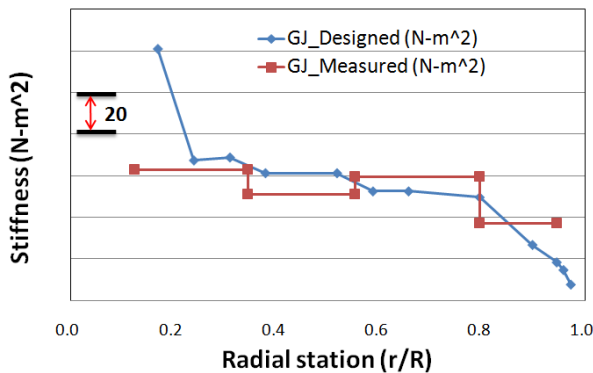


Figure 12. Measured and designed torsion stiffnesses.

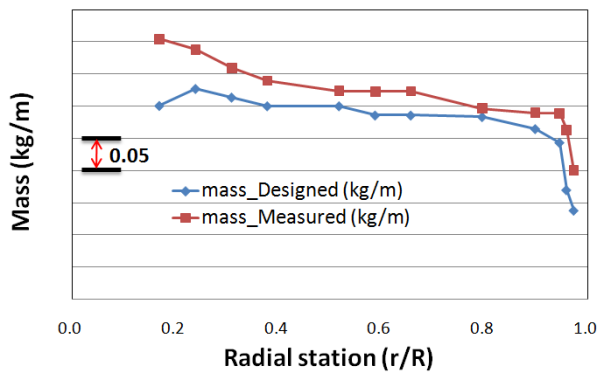


Figure 13. Measured and designed sectional mass distribution.

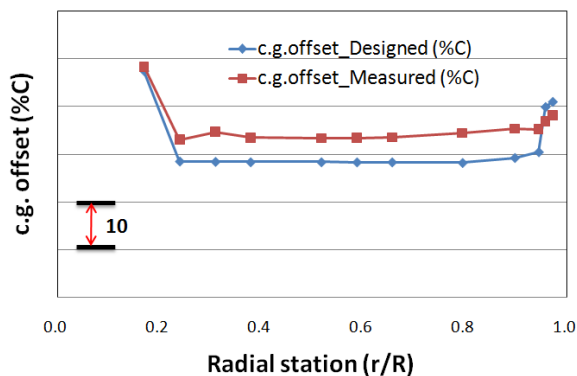


Figure 14. Measured and designed c.g. offsets.

Sectional Mass

In order to obtain blade mass properties at 12 designed locations, 12 sliced pieces were made with 10 mm width. Weight of each piece was measured and then c.g. position was found by balancing the piece at the sharp edge. The measured mass and c.g. offset are compared with designed values in figure 13 and figure 14.

Compared to designed data, measured mass shows 14.7% increase and c.g. offset moves about 3.6% chord aft from leading edge as a whole. The cause of the mass increase is supposed to be the amount of resin absorbed by the foam core, weight of painting which was not considered in designed data, and so on. And the main cause of the c.g. offset movement was slight rearward placement of balancing weight; the circular shape of the balancing weight was not reflected in blade section design, and the actual location of the balancing weight was slightly aft from leading edge.

Non-rotating Frequencies

In order to validate overall properties of the manufactured blade, modal testing of the blade in cantilevered boundary condition was performed. And dynamic characteristics were identified and compared with calculated result. It was not tested at free-free boundary condition, because accelerometers and cable required for mode identification have non-negligible mass compared to model blade. For excluding the effects of sensor's weight, non-contact laser displacement sensor was used for the measurement of displacement response after applying impulsive loading using impact hammer. Twelve locations were selected for measuring frequency response function; it was composed of 6 radial and 2 chordwise locations which can produce flap and torsional mode shapes. For measuring frequency response in lead-lag direction, just single location was utilized, therefore mode shape for lag modes were not identified. The test set-up for modal testing is shown in figure 15.

Modal frequencies and mode shapes were identified using measured frequency response functions. The identified flap mode shapes are shown in figure 16.

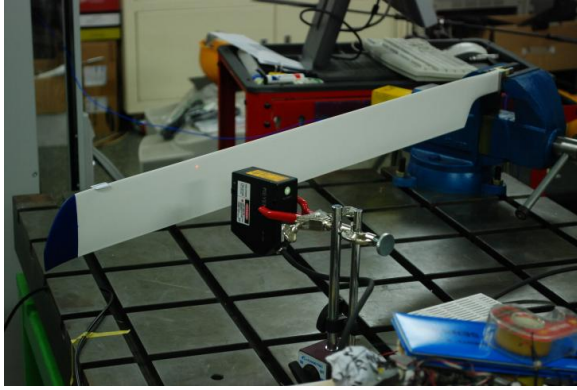


Figure 15. Test set-up for modal testing.

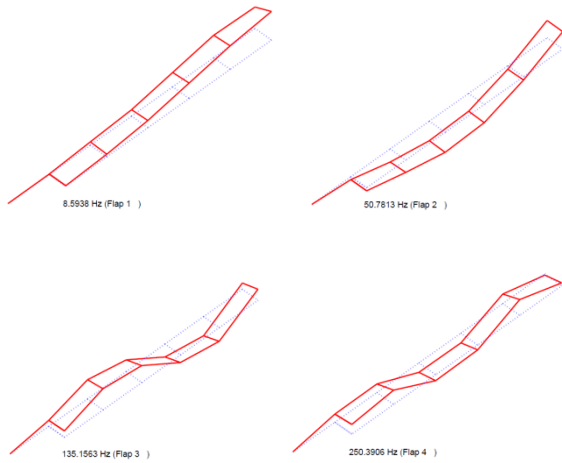


Figure 16. Flap mode shapes.

Table 1. Comparison of non-rotating modal frequencies (Hz).

Mode	Modal Test	Designed Model Analysis
F1	8.6	9.5
L1	34.8	46.7
F2	50.8	55.6
F3	135.8	146.5
T1	204.3	178.2
F4	250.4	276.0
L2	262.5	292.9

The measured modal frequencies are compared with calculated values of designed model in table 1.

The calculated modal frequencies of the designed model are higher in flap and lag modes and lower in torsion mode compared to test result.

Differences in stiffness and mass properties are considered to be the main cause of the discrepancy of modal frequencies.

MODEL UPDATE

As seen in the previous section, measured blade properties are not same to the designed data. In order to construct more actual numerical model representing the scaled model system, model update was performed using test data. First, numerical model was revised using statically obtained stiffness and mass properties, and then non-rotating modal frequencies at cantilevered boundary condition was re-calculated and compared with test data.

Table 2. Non-rotating modal frequencies of updated model (Hz).

Mode	Mass updated	Mass / stiffness updated	Stiffness / inertia tuning
F1	8.9	9.1	8.9
L1	43.9	42.9	42.8
F2	52.0	52.3	51.0
F3	137.3	137.9	134.6
T1	189.7	189.8	204.4
F4	258.0	259.2	252.8
L2	275.0	262.4	262.9

The non-rotating frequencies of the model could be close to the test result by just using the measured mass and c.g. offset. After applying the measured bending stiffness, the 2nd lag mode frequency became closer to the test result. If the bending stiffness and moment of inertia are adjusted, the modal frequencies become closer to the test data except 1st lag mode. The reason for the discrepancy in 1st lag mode frequency is not clearly understood, but it would be helpful to investigate the sectional property variation along the span finely in the transient region from root to the airfoil section. The updated modal frequencies of the numerical model are summarized in table 2, which is calculation result using CAMRAD II.

Rotating frequencies of the updated model were calculated and compared with target and designed models in figure 17. The lowest three modes are

almost same, however the differences in higher modes were reduced after updating the numerical model for matching the static blade properties and dynamic characteristics at non-rotating condition. The updated model is expected to represent the scaled model system more accurately.

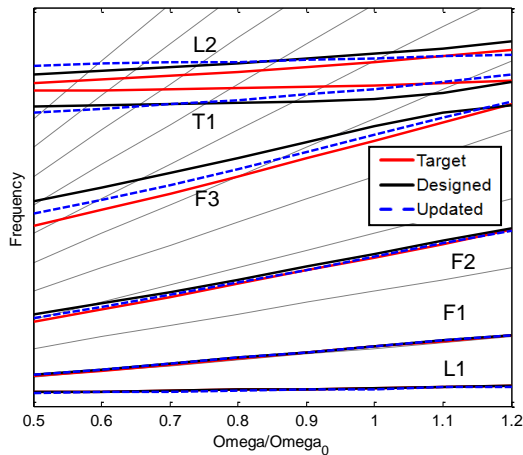


Figure 17. Fanplot of updated model compared with target and designed model.

CONCLUSION

In this study, a dynamically and Mach scaled rotor system was designed and verification process of the blade properties was presented. Uncertainties of the properties can be occurred during design and manufacturing process. Therefore validation of the model properties is necessary. First, bending stiffnesses of the blade were obtained using the strain gauges. The use of strain gauges in measuring bending stiffnesses was useful and reliable. And mass and c.g. position can also be obtained in a simple way. Second, dynamic characteristics of the blade itself were identified through the modal testing in cantilevered condition. Statically obtained stiffness and inertial properties was used to update numerical model to match the modal characteristics. The updated non-rotating modal frequencies of the numerical model became closer to test data. For updating non-rotating modal frequencies, inertial properties were more effective than stiffness properties in reducing the discrepancies of modal frequencies. The updated model will be used for the analysis of wind tunnel test condition.

ACKNOWLEDGEMENT

This study has been partly supported by KHP Dual-Use Component Development Program funded by the Ministry of Knowledge Economy and partly by the Korea Research Council of Fundamental Science and Technology.

REFERENCES

1. Albrecht, Carl O., "Status of Testing and Modeling Techniques for V/STOL Aircraft," AHS Mid-East Region Symposium, Essington, PA, October 26-28, 1972.
2. Singleton, Jeffrey D. and Yeager, William T. Jr., "Important Scaling Parameter for Testing Model-Scale Helicopter Rotors," *Journal of Aircraft*, Vol. 37, No. 3, May-June 2000, pp. 396-402.
3. Yeager, W. T. Jr. and Mantay, W. R., "Correlation of Full-Scale Helicopter Rotor Performance in Air with Model-Scale Freon Data," NASA TN D-8323, 1976.
4. Kim, D.-K., Kim, J.-H., Song, K.-W., Hong, Danbi, and Joo, Gene, "A Correlative Study on Aeroelastic Stability Improvement for Composite Hingeless Hub System by Comparing Analysis and Experimental Results," Presented at the AHS International 62nd Annual Forum, Phoenix, Arizona, May 9-11, 2006.
5. Johnson, W., "CAMRAD II, Comprehensive Analytical Model of Rotorcraft Aerodynamics and Dynamics," Johnson Aeronautics, Palo Alto, CA, 2009.